ARTICLE NO. 77-218

Changing Inclination for Shuttle Payloads

T.M. Spencer* and R. Glickman†
Ball Aerospace Systems Division, Boulder, Colo.
and
G. Porcelli‡
Fairchild Space and Electronics Company, Germantown, Md.

Some payloads using the NASA Shuttle require orbit transfers that change altitude and inclination. This paper treats missions where changing inclination is the dominant requirement, while the altitude increase is small. Two relatively large impulses applied at opposing nodes change both altitude and inclination. Each impulse lies in the plane of the preburn velocity and orbit normal vectors and is nearly aligned with the orbit normal. A small yaw heading offset in this plane provides the tangential velocity component required to change orbit altitude. Accurate aiming is required to prevent in-plane velocity errors from causing large altitude errors. Because altitude is four times as sensitive to tangential as to radial velocity errors, yaw accuracy is most critical. If the spacecraft has adequate Earth sensors and gyroscopes, gyrocompassing is an attractive aiming technique, and altitude errors are minimized by use of roughly equal velocity impulses. A recently developed algorithm uses closed-form covariance combination and propagation to estimate final orbit errors. A novel application of anomalistic superposition permits graphic comparison of each in-plane error source.

Introduction

SOME users of the NASA Space Transportation System (Shuttle) will require orbital parameters different from those readily achievable by the orbiter. The dominant requirement for many of these orbit transfer missions will be to increase altitude or achieve escape velocity. These requirements are similar to those met by the variety of upper-stage vehicles that have been used with expendable boosters. For future Earth-synchronous missions with existing spin-compatible payloads, spin-stabilized upper stages using solid perigee kick motors are attractive.[1] A multimotor-guided Interim Upper Stage (IUS) is being developed to handle large payloads for a variety of future missions.[2]

The Shuttle has increased practical interest in orbit transfer missions that have been uncommon for expendable boosters. One example involves the recovery of a reusable stage vehicle or "tug."[3] Another involves missions requiring large changes in orbit inclination.[4] Past equatorial Earth-synchronous missions included a large 28-deg plane change, but the transfers were strongly affected by the large altitude change. This paper addresses future Shuttle missions that require large plane changes without large altitude changes. For example, early Shuttle Earth survey missions from Cape Canaveral, may require inclinations higher than the orbiter's 57-deg upper limit. Also, inclinations lower than the 28-deg lower limit (without dogleg) are desirable for x-ray, gamma-ray, and EUV astronomy missions to avoid the science-degrading trapped radiation in the South Atlantic Anomaly.

When solid-propellant rocket motors are used, the orbit transfers can be closely approximated as impulses. The literature on optimal impulsive orbit transfers is extensive.[5,6] Considerable attention has also been given to alternative suboptimal transfers between inclined circular orbits.[7,8]

This paper describes an attractive approach for transferring early Shuttle payloads in the 1000-kg class to low-altitude final orbits with plane changes as large as 20 to 30 deg. The comprehensive mission description includes discussion of payload weight optimization, practical hardware limitations, error sensitivity, configuration in the orbiter bay, launch sequence, attitude determination and control, and error analysis approaches. The final design is strongly influenced by engineering realities such as using existing solid rocket motors and stage vehicle components, minimizing error sensitivity, maximizing reliability and flexibility, using satellite attitude control and determination subsystem capabilities, minimizing satellite configuration and constraints, and minimizing orbiter support requirements and launch cost, i.e., bay length. The principal contributions of this paper are in the approaches used to analyze and control final orbit altitude errors which result from an unusual sensitivity to stage vehicle yaw aiming errors.

Performance Considerations

We consider the problem of changing orbit inclination 20 to 30 deg while raising altitude only slightly (from a 185-km nominally circular Shuttle orbit to a 740-km final circular orbit). A velocity impulse ΔV directed roughly along the preburn orbit normal and applied near the ascending or descending node, changes inclination by an amount roughly proportional to $\Delta V/V$, where V is the velocity at the point of application. Rider[7] first observed that there was a potential advantage in using a bielliptical transfer to a higher apogee which reduces V. Three ΔV's are required for bielliptic transfers and a number of analysts soon recognized that, because first-order velocity components along the orbit normal can be produced by aiming the ΔV's slightly out-of-plane with only second-order velocity losses in-plane, the payload-optimal, three-impulse transfer would include three component plane change angles.[6]

For circular initial and final orbits with different altitudes, Baker[8] compared several types of two- and three-impulse transfers using arbitrary apogee altitudes for the latter. For our final-to-initial orbit radius ratio of 1.085 and for various total plane change angles, Fig. 1 shows the total ΔV (normalized with respect to initial circular velocity) vs the ratio of transfer orbit apogee to initial orbit radius. (This figure is derived using the optimization technique described by

Presented as Paper 77-218 at the 23rd Congress of the International Astronautical Federation, Prague, Czechoslovakia, Sept. 25-Oct. 1, 1977; submitted Dec. 21, 1977; revision received Sept. 25, 1978.

Index categories: Earth-Orbital Trajectories; Spacecraft Navigation, Guidance, and Flight-Path Control; Spacecraft Propulsion Systems Integration.

*Chief Astrodynamicist. Member AIAA.
†Senior Systems Analyst, Advanced Programs. Member AIAA.
‡Manager, Guidance and Control Engineer. Member AIAA.

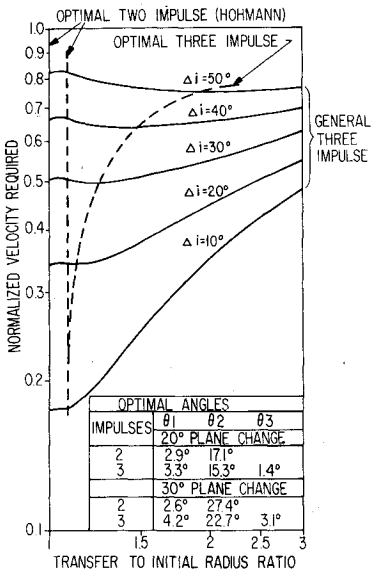

Fig. 1 Comparison of two- and three-burn transfers.

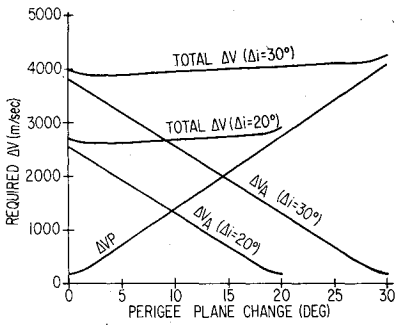

Fig. 2 Required kick velocities.

Baker.[8]) For ratios of 1.000 and 1.085, the three-impulse transfer becomes a two-impulse transfer with the payload-optimal division of plane change angles at perigee and apogee tabulated in the figure. For total plane changes of 20 and 30 deg, the ΔV savings of the more complex three-impulse transfer are only 0.3 and 2%, respectively, and will not be considered further. For plane changes of 40% and more, ΔV savings are significant, and the optimal transfer radius is substantially larger than either circular radius.

Use of existing solid rocket motors and stage vehicle hardware prevents us from achieving a payload-optimal division of our two plane change angles. For total plane change angles of 20 and 30 deg, Fig. 2 shows how required perigee kick velocity ΔV_p, apogee kick velocity ΔV_A, and the total ΔV, vary with perigee plane change angle. The required total ΔV varies roughly 10% over the range of possible perigee plane change angles. The general increase in ΔV with perigee change angle is explained by the fact that the perigee velocities are higher than those at apogee. The rapid increases near extreme perigee change angles are explained by failure to take advantage of a first-order normal velocity component at second-order loss in tangential velocity. For payload weights in the 500- to 1500-kg range, and for selected pairs of existing motors with different impulses from a typical vendor (Thiokol), Fig. 3 shows the total available kick velocity. The perigee plane change angle varies with motor choice and which motor is used at perigee. While payload could be slightly increased (for a given total impulse) by use of a smaller perigee motor and a larger apogee motor, other considerations make this undesirable. These considerations include the spatial distribution of altitude errors and high peak payload accelerations. The solid curve in Fig. 3

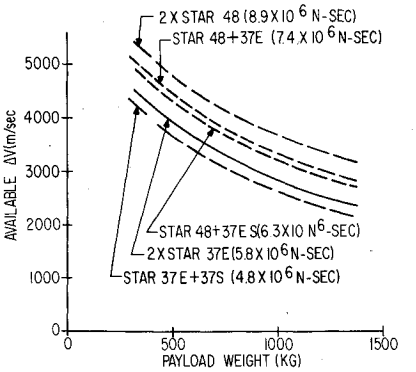

Fig. 3 Available kick velocities.

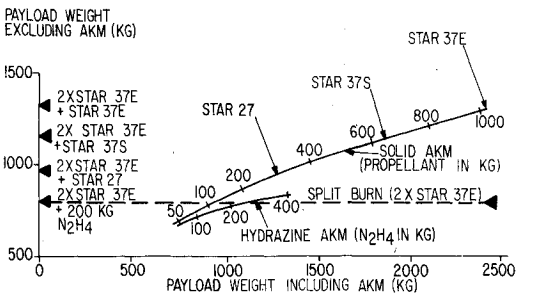

Fig. 4 Usable payload for tandem PKM and one AKM (for $\Delta i = 25$ deg).

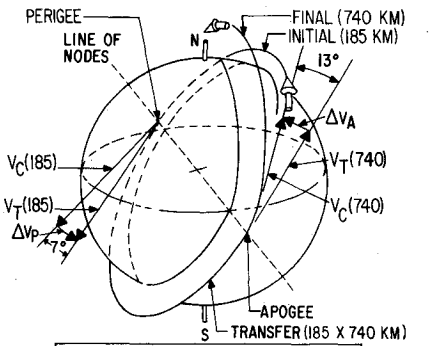

Fig. 5 Two-burn injection geometry.

corresponds to the two STAR 37E motors chosen for our example mission.

The Fairchild tandem stage vehicle that is the basis for our analysis is actually used for a double perigee kick in its existing application. This is followed by a third impulse from an apogee kick motor incorporated in the satellite. While this approach may be attractive for some missions, there are severe payload penalties when most of the plane change is made at perigee. For a 25-deg total plane change and an 800-kg payload, Fig. 4 shows that an apogee kick system with roughly 100 kg of solid or 200 kg of liquid hydrazine propellant is required at apogee to match the performance of our baseline approach in which the tandem burns are split between perigee and apogee. An additional disadvantage of applying a much larger impulse at perigee than at apogee is that final orbit altitude errors would be concentrated near apogee.

Nominal Parameters and Error Sensitivity

The orbit transfer geometry is shown in Fig. 5. We assume that the initial orbit is inclined 56-deg. The objective is to

Table 1 Principal altitude error source sensitivity

One degree	Produces		
Yaw error	ΔV tangential at same apsis	Altitude error at other apsis	Altitude error at midpoint
Perigee	16.7 m/s	64.2 km	32.1 km
Apogee	29.0 m/s	107.8 km	53.9 km
Pitch error	ΔV radial at same apsis	Altitude error at other apsis	Altitude error at midpoint
Perigee	17.1 m/s	0 km	16.5 km
Apogee	29.7 m/s	0 km	30.4 km

achieve as high a final inclination for a 1000-kg satellite as possible using two STAR 37E motors. The allowed altitude variation of the final orbit is 90 km (to keep the satellite well below the Van Allen radiation belts and to control Earth survey fields of view), while the error in final inclination is relatively unimportant. We show the perigee kick at the descending node, but this is arbitrary, and transfer parameters would be the same for a perigee kick at the ascending node, for different initial orbit inclinations, and for transfers that decrease instead of increase orbit inclination.

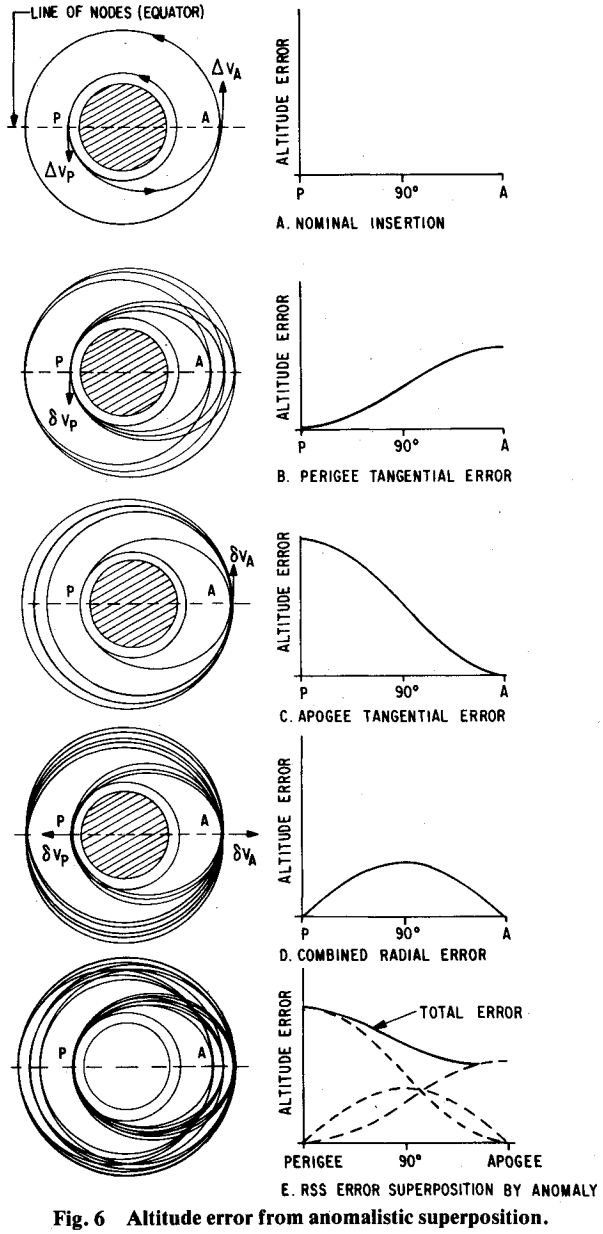

Fig. 6 Altitude error from anomalistic superposition.

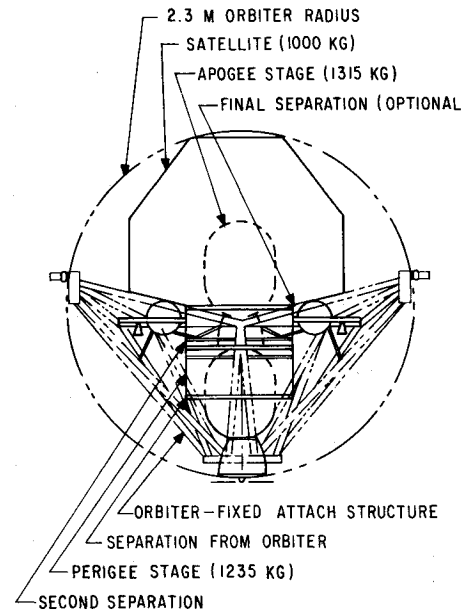

Fig. 7 View looking forward in orbiter bay.

Figure 5 shows that the impulses are nearly aligned with the preburn orbit normals. This means that errors in ΔV magnitude primarily introduce errors in the noncritical final orbit inclination, with only secondary planar errors. For this unusual geometry, yaw aiming errors (in the plane containing the preburn velocity and orbit normal vectors) introduce first-order tangential velocity errors at apogee and perigee, while pitch-aiming errors (in the preburn orbit plane) introduce first-order radial velocity errors. Because altitude variation is four times as sensitive to tangential as to radial velocity errors, yaw aiming errors are most critical. Error sensitivities to nominal 1-deg pitch and yaw aiming errors are given in Table 1. Apogee aiming is most critical because staging identical motors makes the apogee ΔV larger than the perigee ΔV.

Figure 6 graphically illustrates how altitude errors resulting from tangential and radial velocity errors at apogee and perigee propagate with orbital motion. Figure 6a is a planar view of the error-free nominal transfer. For precise error analysis, it is important to project cumulative errors at perigee into the plane of the transfer orbit, and to project cumulative errors at apogee into the plane of the final orbit. The planar views in Figs. 6b, 6c, and 6d clearly show the different distributions (with anomaly) of the absolute value of altitude errors resulting from separately considered error components (error-free burn assumed at opposite apsis except in Fig. 6d).

Assuming that the sources of these velocity errors are statistically independent, the total altitude error should be obtained through some form of root-sum-square (RSS) combination. Differences in spatial distribution cause the RSS of individual peak altitude errors to be an overestimate of the total peak error. We have found that the peak altitude errors can be accurately estimated by the novel technique of RSS combining at each anomaly the individual anomaly-dependent altitude error curves. Figure 6e shows how this "anomalistic superposition" preserves the spatial distribution of the altitude errors.

Configuration

Figure 7 is a view of the space system configuration looking along the axis of the orbiter cylindrical payload envelope. The vertical orientation is preferred over horizontal because it makes more cost-effective use of bay length (only 15 to 20% of the 18.3-m bay is used) while it eliminates the need for a predeployment erection mechanism and the separate jettison mechanism required in cases where the payload envelope is violated prior to deployment.

The stage vehicle is a straightforward structural modification of an existing Fairchild stage vehicle with an enlarged cylindrical section to increase lateral load capability and permit growth to the larger STAR 48 motor. A lateral shelf transmits launch or landing loads to the attach structure and supports the reaction control system (RCS) used for stabilization during solid-motor burns. Considerable RCS fuel growth capacity is available to provide mission length flexibility, postinjection orbit adjustment capability, and a modest increase in the total orbit insertion impulse.

Attitude Control

The satellite envelope in Fig. 7 is highly idealized. While our goal is to minimize satellite configuration constraints, reliability and cost-effectiveness are substantially improved if the satellite attitude determination system can be used for stage vehicle aiming and if the sensors are installed so they have a clear view from the bay. Because each ΔV is nearly along a preburn orbit normal, and Earth survey satellites have preferred orientations with respect to the orbit plane, it is only necessary to mate the satellite so that its preferred orbit normal axis is aligned with the stage vehicle axis and to locate its attitude determination sensors on the "conical" portion of the satellite envelope shown in Fig. 7. These constraints eleminate the need for separate stage vehicle sensors and make predeployment checkout feasible.

For many past missions, spin stabilization has been preferred over three-axis stabilized attitude control because of substantial advantages in simplicity, weight, and reliability. For our inclination-changing mission, the re-aiming between burns (probably without the ground support feasible in Earth-synchronous missions) makes spin stabilization unusually complex. The relatively large ΔV's and tight requirements on aiming accuracy make it necessary to use relatively high spin rates (90 rpm). Unless the kick motors are located on opposite axes of the satellite, the re-aiming angle is nearly 180-deg, and whether the system is precessed between burns or a spin-despin-respin sequence is used, there is no weight advantage. Finally, accurate spin stabilization requires accurate spinup or accurate active precession control, tight constraints on satellite products of inertial, and imposes high centripetal accelerations on large-diameter satellites. For satellites that spin in normal operation, reliability advantages alone may make spin stabilization attractive.

For our mission example we will assume that the satellite has gyroscopes and Earth sensors and that it will be Earth oriented for final orbit operation. This makes three-axes stabilization the preferred approach. The gyroscopes alone can provide attitude hold during burns, while the Earth sensor data can be combined between burns to locate the existing

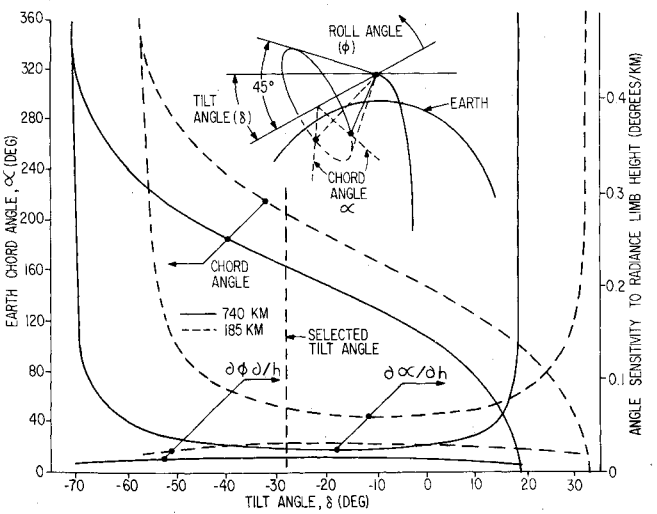

Fig. 8 Earth sensor sensitivity.

Table 2 Mission sequence

1	Orbiter orients satellite for perigee injection to permit gyrocompassing ($Yaw_{bias} = 5.6$ deg)
2	Satellite checkout
3	Continue gyrocompassing ($Yaw_{bias} = 5.6$ deg)
4	Satellite separation and orbiter ΔV (ground monitoring)
5	Continue gyrocompassing ($Yaw_{bias} = 5.6$ deg)
6	Satellite health verification
7	Perigee injection
8	Perigee stage separation
9	Yaw-around 169 deg
10	Continue gyrocompassing ($Yaw_{bias} = 1.6$ deg)
11	Apogee injection
12	Apogee stage separation (optional)
13	Orbit verification and begin on-orbit operations

oribit normal via gyrocompassing. This approach is particularly attractive for inclination-changing burns that must be aimed nearly along the existing orbit normal and must be applied near the equator, where Earth sensor errors due to Earth oblateness and to radiance variation are small.

We assume that the Earth sensors are existing scanning Earth horizon detectors with 90-deg conical scan patterns which permit operation through a large altitude range. Figure 8 shows how the Earth chord angle and the chord angle sensitivity to height variations in the Earth's radiance limb vary with the tilt angle of the scan cone. Performance is relatively insensitive to tilt angle, but there is a well-known error sensitivity increase with decreasing altitude. This effect is partly offset by the fact that larger perigee aiming errors are permissible for the motors we have chosen.

Although high-quality gyroscopes alone might provide an adequate reference throughout the transfer, predeployment gyro alignment must compensate for misalignments between the orbiter bay and its navigation base of 2 deg or more. Schemes that transfer the orbiter reference would add orbiter local vertical reference errors and would require additional equipment or precise orbiter attitude or ΔV maneuvers. Using gyros alone would also reduce reliability and reduce the flexibility to alter the transfer sequence by ground command.

Mission Sequence

The mission sequence listed in Table 2 and depicted in Figs. 9 and 10 is arranged to take advantage of the predeployment checkout inherent with the reusable orbiter while minimizing requirements on orbiter time, attitude control accuracy, and communications support. Assuming that the satellite Earth sensors and communications antenna are properly located, the orbiter can simulate normal satellite operation and align the stage vehicle for the perigee burn by simply rolling one wing down while keeping its nose approximately along the velocity vector (actually a 5.6-deg local yaw angle bias is required for the perigee burn). Rough attitude control to approximately 2 deg for roughly one-quarter orbit is sufficient for a reasonably accurate predeployment gyrocompassing check (orbiter thermal-mechanical distortions make more accurate alignment and checkout difficult).

Satellite deployment follows during the next station pass to allow time to evaluate checkout data and to provide real-time status and warning during deployment via the ground-to-orbiter voice link. The orbiter performs a small ΔV, and the perigee burn is delayed for about one-half orbit to put the orbiter in a safe position during perigee insertion. Proper postdeployment satellite behavior is verified before the burn by onboard or ground comparison of independent sensors. The large angle re-aiming maneuver between burns is executed about the satellite yaw axis. Earth survey satellites are typically capable of yawing around the nadir vector (to keep the Sun in a preferred body-fixed hemisphere) and Fig. 10 shows that the Earth sensors maintain Earth-lock throughout

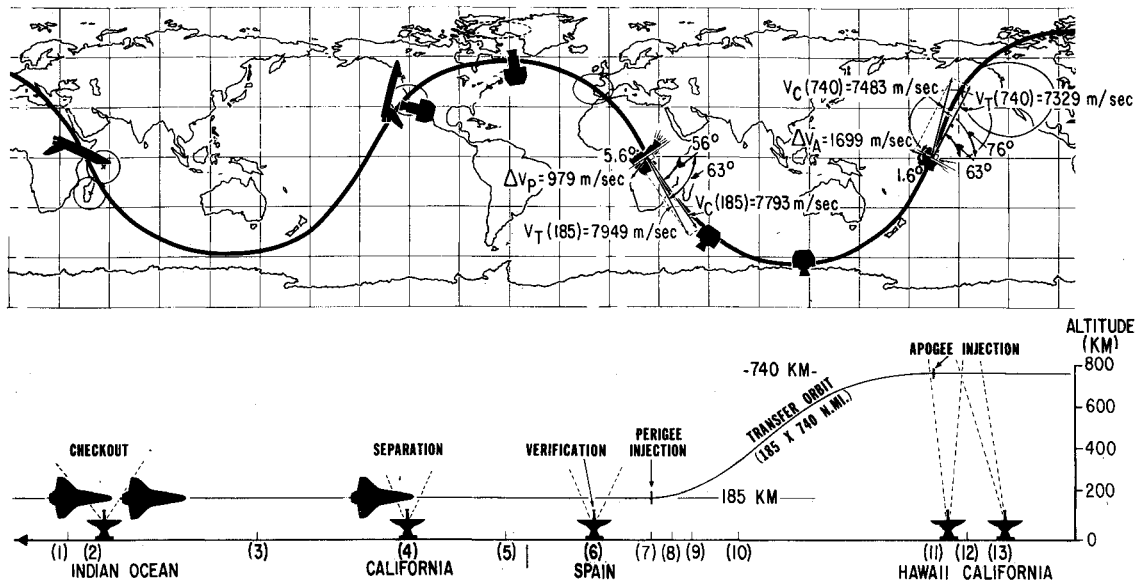

Fig. 9 Typical mission sequence.

the entire checkout-deployment-transfer sequence. This increases sequence reliability.

The guided control approach with gyrocompassing provides excellent mission sequence flexibility. If a burn is inhibited for any reason, the system can be rapidly re-aimed by ground command, and the burn can be rescheduled near an appropriate later nodal crossing.

Covariance Error Analysis

Our recently developed covariance matrix analysis program uses a deterministic formulation to compute the orbit insertion errors in a two-stage noncoplanar transfer, given the covariance matrices of the source errors (see Table 3). The algorithm for matrix combination and propagation is shown schematically in Fig. 11. Inputs to the algorithm are the matrices C_{PS}, C_{P0}, C_{AS}, T_{PS}, T_{P0}, T_{PA}, T_{AS}, T_{AH}, and T_{FS}. The covariance matrix C_{P0} describes the initial orbiter errors. The covariance matrices C_{PS} and C_{AS} are stage vehicle dependent. The matrices T_{PS}, T_{P0}, T_{PA}, T_{AS}, T_{AH}, and T_{FS} are derived either from geometrical considerations associated with the velocity vector composition through the plane changes (transfer matrices T_{PS}, T_{P0}, T_{AS}, T_{AH}), or from Keplerian orbital mechanics (state transition matrices T_{PA} and T_{FS}). In all matrices, nominal values or orbital parameters, velocity increments, and angular values of the plane changes associated with a given transfer mission appear in the expressions defining their elements. A derivation of all of these matrices and a complete description of the algorithm is given by Porcelli and Vogel.[9]

The orbit insertion errors for the "allowed" aiming errors in our mission example are displayed in the "modified" final orbit covariance matrices, C_{FS} and C_{FE} (Tables 4 and 5). The symmetric covariance matrices have been modified by replacing the covariance elements above the diagonal with correlation coefficients. This modification provides additional insight. The bottom lines of each table give the 3σ errors associated with the variances along the matrix diagonal. The overall 3σ errors for allowed aiming errors are 0.01 for eccentricity, 67 km for semimajor axis, and 0.18 deg for inclination. (The 3σ errors for "expected" aiming errors are 0.004 for eccentricity, 27 km for semimajor axis, and 0.12 deg for inclination.) The altitude errors are next examined using anomalistic superposition.

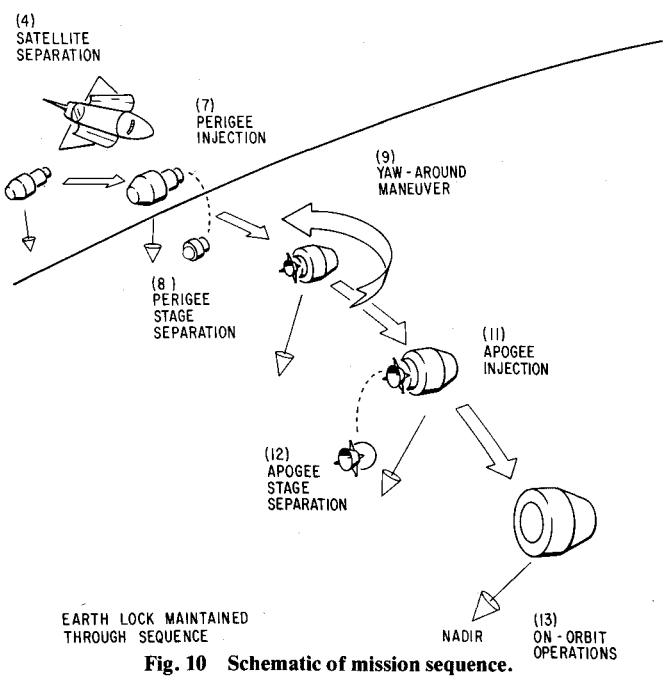

Fig. 10 Schematic of mission sequence.

Table 3 3σ error sources

Shuttle orbit errors at perigee burn:	
Geocentric radial distance	±500 m
Inertial velocity magnitude	±4 m/s
Path angle (from outward vertical)	±0.05 deg
Velocity azimuth	±0.05 deg
Correlation coefficients:	
Radius/velocity	−0.3
Radius/path angle	−0.8
Velocity/path angle	+0.4
All other coefficients	Negligible
Errors during perigee burn:	
Impulse error	±0.75%
Propellant grain temperature variation	±2°C
Pitch/yaw attitude errors (allowed)	±1.5 deg
(expected)	±0.4 deg
Ignition timing error	±30 s
Errors during apogee burn:	
Impulse error	±0.75%
Propellant grain temperature variation	±5°C
Pitch/yaw attitude errors (allowed)	±0.8 deg
(expected)	∓0.4 deg
Ignition timing error	±30 s

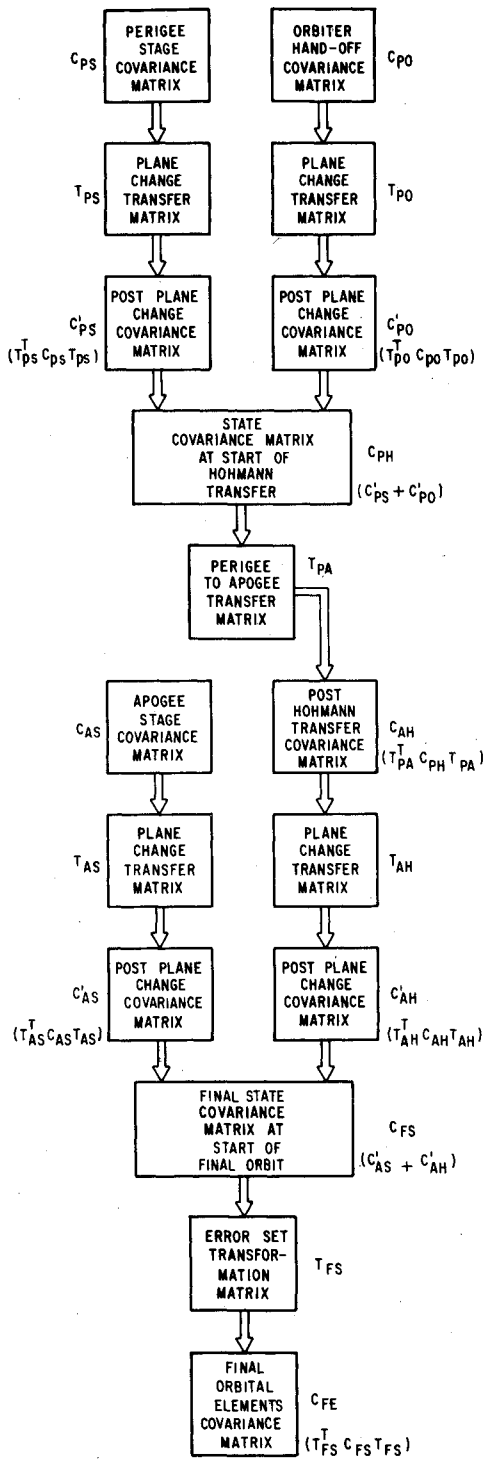

Fig. 11 Covariance matrix combination and propagation.

Anomalistic Superposition of Altitude Errors

Both final covariance matrices (Tables 4 and 5) contain a comprehensive description of planar orbit errors. Unfortunately, useful engineering data are buried within these matrices and some data are only accessible through comparison with intermediate matrices and suppression of some error sources. To interpret the combination of individual errors, it is useful to introduce apsidal and transverse eccentricity "components" (referenced to the apsidal line of the transfer orbit) and to visualize the effect of spatial distribution of individual errors by anomalistic RSS superposition. If proper care is exercised in its application, this earlier described technique could be used in place of covariance analysis to obtain reasonably accurate planar error estimates. Here, we apply it to interpret the results of the covariance analysis.

The first problem we consider is that of defining the allowed perigee and apogee aiming errors that just meet the ±90-km altitude accuracy requirement (under the assumption that the other errors in Table 3 are fixed beyond our control). This takes some iteration of assumed aiming errors. Anomalistic superposition provided sufficient insight to permit the result in Fig. 12 to be obtained in the second iteration. Figure 12 shows that larger pitch errors could be allowed before the combined pitch error contribution would have any effect on the peak altitude error. For small perturbations to our nearly circular orbits, the propagation of the cumulative perigee tangential velocity error in Fig. 12 (assuming no apogee errors) is approximately

$$|\Delta h_{TP}(\theta)| \approx |\Delta h_a| (1-\cos\theta)/2 = |\Delta R(F)| (1-\cos\theta)/2$$

where the altitude error at the apogee anomaly Δh_a is the radius error at transfer orbit apogee $\Delta R(F)$ in Table 4, and θ is the anomaly (angle) from perigee. The propagation of the cumulative apogee tangential velocity error (assuming no perigee errors) is approximately

$$|\Delta h_{TA}(\theta)| \approx |\Delta h_p| (1+\cos\theta)/2$$

where

$$|\Delta h_p| \approx \{ [\,|\Delta A(F)| + A(F)\Delta E(F,1)\,]^2 - \Delta h_a^2 \}^{1/2}$$

is the altitude error at the transfer orbit perigee, and where the semimajor axis error $\Delta A(F)$, and apsidal eccentricity $\Delta E(F,1)$, are from Table 5. The cumulative effect of the radial velocity errors at perigee and apogee is expressed via the transverse eccentricity component $\Delta E(F,2)$ from Table 5 as

$$|\Delta h_R(\theta)| \approx |\Delta h_t| \sin\theta = A(F)\Delta E(F,2)\sin\theta$$

where Δh_t is the altitude error midway between perigee and apogee.

Since the three curves in Fig. 12 are the separate effects of uncorrelated error sources, the estimate of the total final orbit

Table 4 Final state covariance matrix C_{FS}

Radial position $\Delta R(F)$, m	Normal position $\Delta N(F)$, m	Radial velocity $\Delta V(F,R)$, m/s	Tangential velocity $\Delta V(F,T)$ m/s	Normal velocity $\Delta V(F,N)$, m/s
9.3298E+008	0.0000E+000	3.8261E−001	−9.4817E−001	−7.2688E−001
0.0000E+000	0.0000E+000	0.0000E+000	0.0000E+000	0.0000E+000
1.4308E+005	0.0000E+000	1.4989E+002	−3.6281E−001	−2.7548E−001
−7.1279E+005	0.0000E+000	−1.0932E+002	6.0573E+002	7.8335E−001
−1.7282E+005	0.0000E+000	−2.6252E+001	1.5006E+002	6.0585E+001
		3σ sigma errors		
9.1634E+004	0.0000E+000	3.6729E+001	7.3834E+001	2.3351E+001

Table 5 Final orbit elements covariance matrix C_{FE}

Semimajor axis $\Delta A(F)$, m	Apsidal eccentricity $\Delta E(F, 1)$	Transverse eccentricity $\Delta E(F, 2)$	Inclination $\Delta I(F)$, deg	Ascending node $\Delta\Omega(F)$, deg
4.9987E + 008	−2.1556E − 002	2.8550E − 001	−3.4530E − 001	0.0000E + 000
−1.3766E + 000	8.1589E − 006	−2.6082E − 001	7.1219E − 001	0.0000E + 000
1.0444E + 001	−1.2189E − 006	2.6770E − 006	−2.7548E − 001	0.0000E + 000
−4.6011E + 002	1.2124E − 004	−2.6863E − 005	3.5521E − 003	0.0000E + 000
0.0000E + 000	0.0000E + 000	0.0000E + 000	0.0000E + 000	0.0000E + 000
		3σ sigma errors		
6.7074E + 004	8.5691E − 003	4.9084E − 003	1.7880E − 001	0.0000E + 000

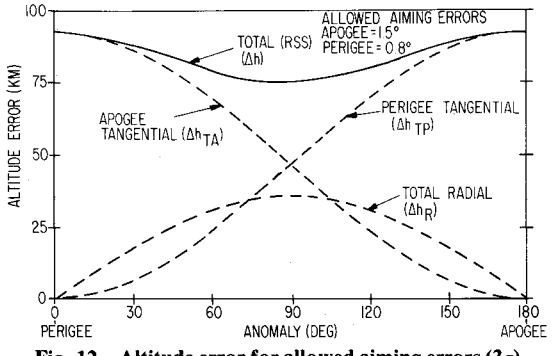

Fig. 12 Altitude error for allowed aiming errors (3σ).

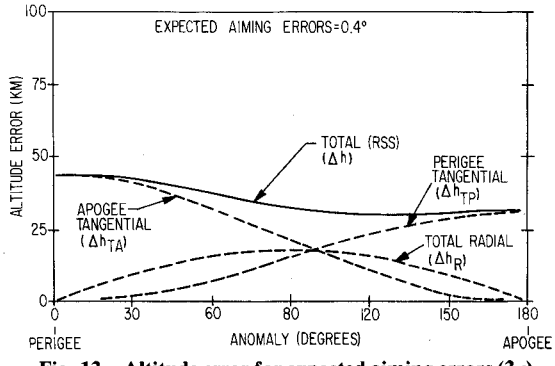

Fig. 13 Altitude error for expected aiming errors (3σ).

altitude variations is given by

$$\Delta h^2(\theta) \approx \Delta h^2_{TP}(\theta) + \Delta h^2_{TA}(\theta) + \Delta h^2_R(\theta)$$

We have constrained max. $|\Delta h(\theta)|$ to just meet the 90-km requirement. Note that this error is the combined effect of the previously mentioned eccentricity error of 0.01 with a semimajor axis error of 67 km.

With the chosen gyrocompassing attitude determination approach and with moderately accurate three-axis limit-cycle attitude control, the expected 3σ pitch and yaw aiming errors are roughly 0.4 deg at both perigee and apogee. Figure 13 shows the spatial distribution of the expected altitude error and makes it clear that somewhat larger perigee aiming errors would not affect the expected peak altitude error of about 40 km.

Summary

Relatively tight attitude control is required for relatively large plane changes between low-altitude orbits. The unusual transfer geometry makes yaw aiming most critical. For satellites with adequate gyros and Earth sensors, an existing stage vehicle can be slightly modified and integrated with the orbiter to provide a cost-effective, reliable, and flexible transfer mission. The complementary techniques of closed-form covariance error analysis and anomalistic superposition provide accurate error estimates and a clear visualization of the relative importance of individual error sources.

References

[1] Aerospace Corporation, "Spinning Solid Upper Stage for Delta and Atlas/Centaur Class Missions," (Study 2.6) Final Report, Aerospace Corporation, Aerospace Rept. ATR-76(7377-01)-01, Vols. I and II.

[2] "Special Report: Space Shuttle, Transportation System of the Future," *Aviation Week and Space Technology,* Vol. 105, Nov. 8, 1976, pp. 36-154.

[3] Borsody, J., "Performance of a Recoverable Tug for Planetary Missions Including Use of Perigee Propulsion and Corrections for Nodal Regression," AIAA Paper 76-809, AIAA/AAS Astrodynamics Conference, Aug. 18-20, 1976.

[4] Betts, J.T., "Optimal Three-Burn Orbit Transfer," *AIAA Journal,* Vol. 15, June 1977, pp. 861-864.

[5] Marchal, C., "Optimisation des trajectoires spatiales (Synthese)," Paper AIF-76-010, XXVIIth Congress of International Astronautical Federation, Oct. 10-16, 1976.

[6] Gobertz F.W. and Doll, J.R., "A Survey of Impulsive Trajectories," *AIAA Journal,* Vol. 7, May 1969, pp. 801-834.

[7] Rider, L., "Characteristic Velocity Requirements for Impulsive Thrust Transfers between Noncoplanar Circular Orbits," *ARS Journal,* Vol. 31, March 1961, pp. 345-351.

[8] Baker, J.M., "Orbit Transfer and Rendezvous Maneuvers between Inclined Circular Orbits," *Journal of Spacecraft and Rockets,* Vol. 3, Aug. 1966, pp. 1216-1220.

[9] Porcelli, G., and Vogel, E., "Two-Impulse Orbit Transfer Error Analysis via Covariance Matrix," AIAA Paper 79-0256, Aerospace Sciences Meetings, New Orleans, La., Jan. 15-17, 1979.